

Enhancement of Bag-of-Features Method for Classification of Histopathological Images

Presented by:
Raju Pal (PhDI-1443008)

Under Guidance of :
Dr. Mukesh Saraswat



Department of Computer Science
Jaypee Institute of Information Technology, Noida

December 16, 2019

Introduction

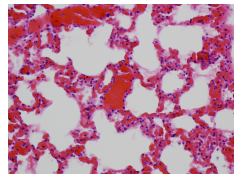
- Image Classification

- Medical image analysis
 - Histopathological image analysis

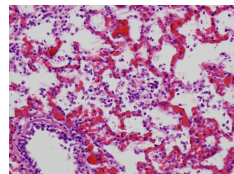
- Histopathological Analysis → Study the changes in tissue images

- Application Areas:

- ① Counting of various cells (i.e. Leukocytes, RBC etc.) in histopathological images
- ② Identification of inflamed and healthy histopathological images



(a) Healthy tissue



(b) Inflamed tissue

Figure 1: Histopathological Images [1]



Motivation

Problems Associated with Manual Histopathological Analysis [21, 50]

- A shortage of dedicated trained pathologists
- The individual microscope observations are biased in nature
- Wide natural biological variability across tissue sections
- Time consuming process



Figure 2: Manual analysis of histopathological images [73]

Challenges Associated with Automated Histopathological Analysis [21, 50]

- Lack of labeled image dataset
- Histopathological images have complex morphological structure
- Classification accuracies are still adequate

Automated Histopathological Image Classification

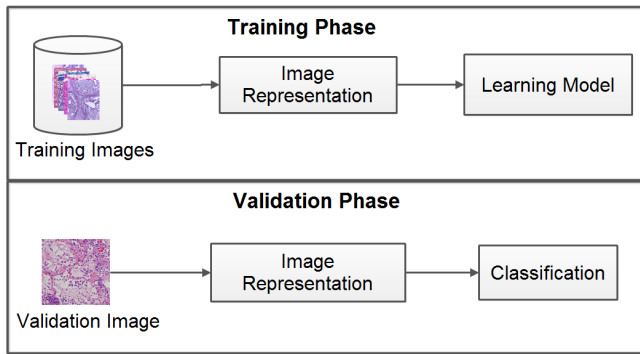


Figure 3: General work flow of an automated histopathological image classification

Automated Histopathological Image Classification

- On the basis of Image representation, Histopathological Image Classification methods can be divided into three categories [22]:
 - Statistical-based methods
 - Extract handcrafted features like color, morphological structures [15], nuclei distribution [72], and many more
 - Not able to express the complex visual morphology in histopathology images [55] [22]
 - Learning-based methods
 - Use different machine learning techniques to automatically extract the features that are used to represent the data in a more meaningful and collective manner
 - Auto-encoders [14, 71], restricted Boltzmann machines [46, 10], Convolutional Neural Network [40, 23], and many more [6, 58, 7]
 - Large training dataset is required for training
 - Require more memory and high computational time [22]
 - Mid-level representation based methods
 - Transforming low-level descriptors into a global and richer image representation
 - The NeTra toolbox [39], RETIN system [16], Bag of features (BOF) [9]
 - Kumar et al. [27] validated that Bag of feature representations outperforms other representation for histopathological image classification



Bag of Features based Histopathological Image Classification System

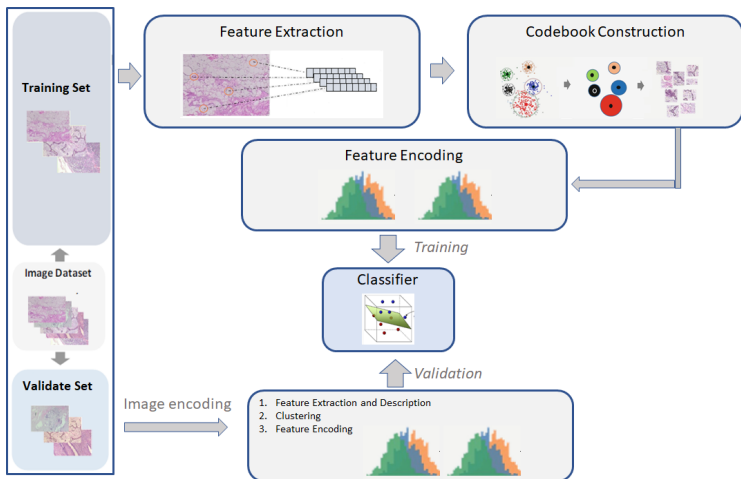


Figure 4: Bag-of-feature approach for Histopathological image classification [9]



Features Extraction

- Visual features aim to describe the most relevant information to feed a specific Machine Learning (ML) algorithm

Table 1: Categorization of Features used in Bag of features methods [32]

Category	Classification	Comments	Methods
Blob detection (Interest Point)	Partial Differential Equations based	Based on the partial differentiation on Gaussian scale spaces	LoG [49], DoG [56], DoH, Hessian-Laplacian [51], SIFT [13, 17], SURF [56, 64], KAZE [59]
	Template based	Based on binary comparison and decision tree; computationally fast	BRISK [31], FREAK [47], ORB [64]
Learned Features	Deep Features	High-level abstractions obtained from raw images	DNN [12, 4], SSAE [70], CNN [14]

- SIFT and SURF features are robust to scale, rotation, and illumination changes while ORB is a computationally fast method [5]
- However, due to complex morphological structures of histopathological images these methods generate high dimensional feature vectors



Codebook Construction

- The extracted features are quantized into different clusters to find the visual words.
The collection of visual words is known as **codebook**

Table 2: Various codebook construction methods used in Bag of features [25]

Category	Methods	Comments
Partitional methods	K-means [25, 9, 60], FCM, GMM [60]	Generates non-uniform coding (biased towards dense regions) optimal codebook size (K) is unambiguous
Hierarchical methods	Agglomerative clustering [2, 30], Mean Shift [19]	These methods can not be applied to large datasets or histology images due to high computational cost
Meta-heuristic methods	PSO, GSA, DE, CSMO [28]	Used to find optimal visual words based on some objective function defined over compactness and separation Computationally expensive



Feature Encoding

- Each image is encoded in terms of visual words by different **feature encoding methods**

Table 3: Various encoding methods used in Bag of features [24, 54]

Type	Methods	Comments
Voting based	Hard voting (HV), Soft-assignment (SA), Localized SA, Salient coding (SC), Group salient coding (GSC)	Describe distribution of features with a histogram which carries the occurrence of information of codewords
Reconstruction based	Orthogonal matching pursuit (OMP), Sparse coding (SC), Locality-constrained Linear Coding (LLC), Local Coordinate Coding (LCC)	Use a small part of codewords to describe each feature via solving a least-square-based optimization problem with constraints on codewords
Super vector based	Local Tangent-based Coding (LTC), Super Vector Coding (SVC), Fisher Vector, Vector of Locally Aggregated Descriptors (VLAD)	Estimate the distribution of features with GMM consisting of weights, means, and covariance matrix of multiple Gaussian distributions, each of which reflect one pattern of feature

- All encoding methods use single feature to encode the images and this can be extended for more than one feature

Classification

- The classifier identifies or categorizes image components based on the extracted features

Table 4: Popularly used classification methods for Histopathological Image Classification

Classifier	Comments	References
Random Forest	Creates a set of decision trees and aggregates the votes from different decision trees to decide the final class of the test image	[63] [66]
Logistic Regression	A Linear classifier which uses the calculated logits (score) to predict the target class	[68] [23]
Support Vector Machine	A discriminative classifier formally defined by a separating hyperplane which are further used to categorize new test images	[62] [29] [57]
Linear Discriminant Analysis	Find a linear combination of features that characterizes or separates two or more classes of images	[35]
Bayesian Classifier	A probabilistic model where the classification is a latent variable that is probabilistically related to the observed variables	[62] [67] [20]

Research Gaps

① High dimensional keypoint descriptors

- Histopathological images contains various morphological variabilities and structures, due to which high dimensional keypoint descriptors are generated
- This make codebook construction computationally expensive and prompt to generate irrelevant visual words
- No method has been reported to select the relevant keypoints from the extracted high dimensional keypoint descriptors in BOF method for histopathological images

② The generated visual words are biased towards densest regions in descriptor space and thus failing to code other informative regions

③ Existing meta-heuristic based visual word generation methods are computationally expensive

④ Existing feature encoding methods consider only single image feature to encode an image



Objectives

- ① To design a new keypoint selection method for finding discriminative and relevant features for codebook construction
- ② To design an efficient meta-heuristic based codebook generation method to reduce the effect of dense regions of histopathological images
- ③ To design a computationally efficient and effective codebook generation method for finding the relevant visual words
- ④ To design an efficient feature encoding method by incorporating the merits of two different features descriptors for the better image representation



Grey Relational Analysis based Keypoint Selection Method

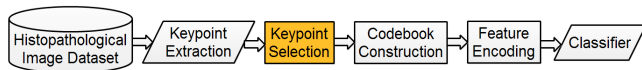


Figure 5: Flow chart of the BOF method

- In histopathological images, the extracted feature vectors are of high dimension
- An efficient keypoint selection method can improve the performance
- Various keypoints selection methods are: IKS [34], ICF [8], IB3 [3]
- These keypoints selection methods are based on Euclidean similarity which increases the computational cost when applied on high dimensional data [11]
- In this work, grey relational analysis (GRA) based keypoint selection method is presented which is an efficient similarity measure



Grey Relational Analysis based Keypoint Selection Method (GKS)

Initial parameters

- ① Let P is the number of keypoints detected from the training set
- ② Select a set of n reference keypoints using approximate K-means ($X_o = X_{r1}, X_{r2}, \dots, X_{ri}, \dots, X_{rn}$)
- ③ Each reference point is a u dimensional vector ($X_{ri} = \langle X_{ri}(1), X_{ri}(2), \dots, X_{ri}(u) \rangle$)
- ④ The set of remaining $m = P - n$ keypoints are considered as comparative keypoints ($X_c = \langle X_{c1}, X_{c2}, \dots, X_{cm} \rangle$)

Similarity measure using grey relational analysis

- ① GRA uses the grey relational coefficients (GRC) to describe the trend relationship between the comparative and reference keypoints. The GRC value, between i^{th} keypoint of X_o and m keypoints of X_c is given is by

$$GRC(X_{r1}(u), X_{cj}(u)) = \frac{\Delta_{min} + \xi \Delta_{max}}{\Delta_{r1j}(u) + \xi \Delta_{max}},$$

where, $\xi \in (0, 1]$ is a random number and $\Delta_{r1j}(u)$ is computed by $|X_{r1}(u) - X_{cj}(u)|$ for $j = 1, 2, \dots, m$

- ② Then, grey relational grade (GRG) is used to find overall similarity degree between the reference keypoint X_{r1} and comparative keypoints X_{cj}

$$GRG(X_{r1}, X_{cj}) = \frac{1}{m} \sum_{t=1}^m [GRC(X_{r1}(t), X_{cj}(t))]$$

- ③ When the value of GRG approaches 1, the two sequences are 'more closely similar'. When GRG approaches a value 0, the two sequences are 'more dissimilar'.

Grey Relational Analysis based Keypoint Selection Method (GKS)

Keypoint selection

- ④ The above computation is performed to find the highly similar points with cluster center and eliminate $s\%$ of the keypoints from each cluster whose GRG values are higher, in their corresponding cluster. Here, s is termed as shrinking threshold.
- ⑤ Repeat the steps 1 to 4 till the remaining keypoints are greater than n and add the last set (having n points only) of cluster centers to the selected keypoints set.
- ⑥ Use the selected keypoints set as input to the next phase of BOF i.e., codebook construction.



Experimental Results

- ① The proposed keypoint selection method has been validated against other state-of-the-art keypoint selection methods, namely IB3, IKS1, and IKS2 [34]
- ② Two standard **histopathological image datasets** are considered for the classification task
 - ① **ADL Dataset** [65]
 - Hematoxylin and Eosin (H&E) dye is used for staining
 - Scanning at $40\times$ optical magnification
 - Three bovine organs - Kidney, Lung, Spleen (healthy/inflamed)
 - 120 images per condition per organ
 - ② **Blue Histology Dataset** [63]
 - Contains images of four tissues, namely epithelium, connective, muscular, and nervous
 - Each image category contains 101 tissue images
 - Various staining methods are used - H&E, Trichrome, Elastin, Methylene blue, Immunocytochemistry, Carbocyanine, etc.
- ③ K-means is used to generate the visual words from the selected keypoints which are further encoded by vector quantization method
- ④ The encoded images with labels are used to train support vector machine
- ⑤ The performance of GKS method has been evaluated in terms of
 - Number of selected keypoints
 - Average computation time
 - Confusion matrices
 - Classification accuracy
 - Radar charts

Experimental Analysis: Keypoint Selection

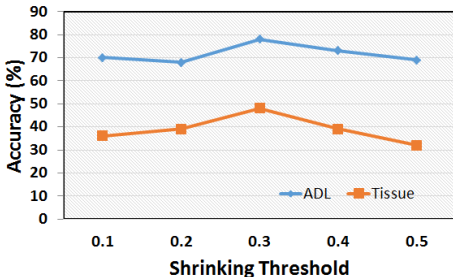


Figure 6: Classification accuracy on validation set using the GKS method with different shrinking threshold values

Table 5: Number of selected keypoints returned by IB3, IKS1, IKS2, and GKS on considered datasets along with their average computational cost.

Methods	Number of keypoints		Average computational time (in hours)	
	ADL	Blue histology	ADL	Blue histology
Without keypoints selection	4177920	158720		
IB3	626688 (85%)	57139 (64%)	85.71	15
IKS1	1100000 (74%)	65948 (59%)	40	7
IKS2	2003000 (52%)	70312 (56%)	8	3.5
GKS	203000 (95%)	51000 (68%)	4	1

Experimental Analysis: Classification performance

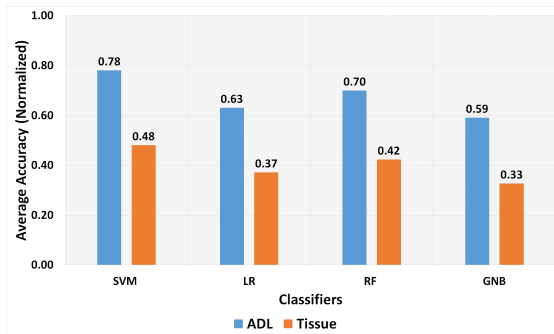


Figure 7: Classification accuracy on validation set using the GKS method with different classifiers

Experimental Analysis: Classification performance - ADL Dataset

		Predicted					
		KI	KN	LI	LN	SI	SN
Actual	KI	0.35	0.15	0.05	0	0	0.5
	KN	0.8	0.1	0	0	0	0.25
	LI	0.1	0.25	0.4	0.15	0	0
	LN	0	0.55	0.1	0.5	0.2	0
	SI	0	0.1	0	0.5	0.1	0.65
	SN	0	0	0	0	0.05	0.2

(a) IB3

		Predicted					
		KI	KN	LI	LN	SI	SN
Actual	KI	0.6	0.35	0	0.05	0	0
	KN	0.15	0.6	0	0.1	0.05	0.1
	LI	0.05	0.15	0.4	0.3	0.1	0
	LN	0	0	0	1	0	0
	SI	0	0	0	0	0.6	0.4
	SN	0	0.05	0.05	0	0.05	0.85

(b) IKS1

		Predicted					
		KI	KN	LI	LN	SI	SN
Actual	KI	0.8	0.15	0.05	0	0	0
	KN	0.35	0.65	0	0	0	0
	LI	0.1	0.25	0.5	0.15	0	0
	LN	0	0	0	1	0	0
	SI	0	0.1	0	0	0.25	0.65
	SN	0	0	0	0	0.05	0.95

(c) IKS2

		Predicted					
		KI	KN	LI	LN	SI	SN
Actual	KI	0.85	0.15	0	0	0	0
	KN	0.05	0.8	0	0	0.15	0
	LI	0.2	0.05	0.5	0.1	0.1	0.05
	LN	0	0	0	1	0	0
	SI	0	0.1	0	0	0.7	0.2
	SN	0	0.05	0	0	0.1	0.85

(d) GKS

Figure 8: The confusion matrices for the ADL dataset, generated by (a) IB3, (b) IKS1, (c) IKS2, and (d) GKS based classification methods.



Experimental Analysis: Classification performance - Blue Histology Dataset

IB3		Predicted			
		CT	ET	MT	NT
Actual	CT	0.25	0.3	0.4	0.05
	ET	0.25	0.2	0.35	0.2
	MT	0.35	0.1	0.1	0.25
	NT	0.4	0.3	0.3	0.1

(a) IB3

IKS1		Predicted			
		CT	ET	MT	NT
Actual	CT	0.45	0.1	0.4	0.05
	ET	0.05	0.5	0.35	0.1
	MT	0.35	0.1	0.3	0.25
	NT	0.4	0.3	0.1	0.2

(b) IKS1

IK2		Predicted			
		CT	ET	MT	NT
Actual	CT	0.5	0.2	0.3	0
	ET	0.35	0.3	0.25	0.1
	MT	0.15	0.05	0.7	0.1
	NT	0.5	0.1	0.2	0.2

(c) IKS2

GKS		Predicted			
		CT	ET	MT	NT
Actual	CT	0.75	0.1	0.15	0
	ET	0.45	0.35	0.2	0
	MT	0.2	0.05	0.75	0
	NT	0.6	0.15	0.2	0.05

(d) GKS

Figure 9: The confusion matrices for the Blue histology dataset, generated by (a) IB3, (b) IKS1, (c) IKS2, and (d) GKS based classification methods.

Classification Performance

Table 6: Comparative analysis of the proposed GKS based BOF method with other considered methods in terms of average accuracy. The best results are in bold

Category	IB3	IKS1	IKS2	GKS
ADL Dataset	27	68	69	78
Blue Histology	17	36	43	48

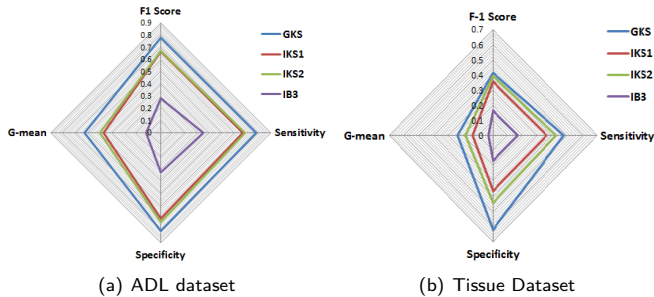


Figure 10: Radar Charts for average results obtained for SVM classifier on a) ADL dataset and b) Tissue image dataset by considering F-1 score, sensitivity, specificity, and G-mean

Research contribution

- A new Grey relational analysis based keypoints selection technique is proposed and used in BOF framework for finding the relevant keypoints
- The proposed method selects minimum number of keypoints and increases the classification accuracy by 13% and 11% for ADL dataset and Blue Histology dataset respectively



Objectives

- ① To design a new keypoint selection method for finding discriminative and relevant features for codebook construction
- ② To design an efficient meta-heuristic based codebook generation method to reduce the effect of dense regions of histopathological images
- ③ To design a computationally efficient and effective codebook generation method for finding the relevant visual words
- ④ To design an efficient feature encoding method by incorporating the merits of two different features descriptors for the better image representation



Codebook Generation

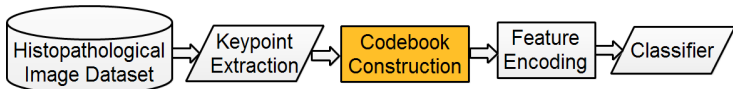


Figure 11: Flow chart of the BOF method

- Codebook is the collection of prominent visual words
- Partitional clustering methods are used to generate visual words which are biased towards densest regions in histopathological images
- Various meta-heuristics based methods are used to generate optimal set of visual words
- In literature, it has been stated that Biogeography-based Optimization (BBO) outperforms other meta-heuristics in computer vision applications [38]
- However, BBO also suffers from the following demerits [37, 33]:
 - Single feature migration property
 - Poor population diversity
 - BBO may get stuck in local optima



Codebook Generation

- Two new variants of BBO, namely **improved biogeography-based optimization** (IBBO) and **spiral biogeography-based optimization** (SBBO) are proposed
- The proposed methods are used to generate the optimal visual words



Biogeography-based Optimization

- BBO [61] is an evolutionary algorithm which is inspired from the mathematical model of island biogeography

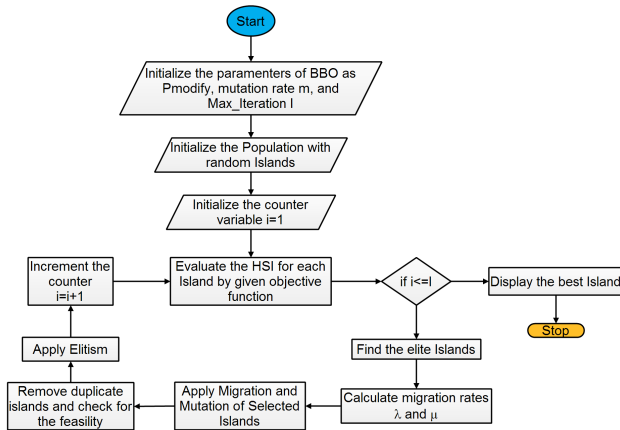


Figure 12: Flow chart of BBO algorithm



Biogeography-based Optimization

Migration Operator [36]

```

1: Input: Let  $\lambda_i$  and  $\mu_i$  are the immigration rate and
   emigration rate of  $i^{th}$  island ( $island_i$ ) respectively.
2: Each island has  $d$  suitability index variables (SIVs)
   i.e. ( $SIV_1$ ,  $SIV_2$ , ...,  $SIV_d$ )
3: Let  $P_{modify}$  is the island modification probability.
4: Output: A population of  $m$  modified islands.
5: for  $i = 1$  to  $m$  do
6:   if  $rand < P_{modify}$  then
7:     continue;
8:   end if
9:   for  $j = 1$  to  $d$  do
10:    if  $rand < \lambda_i$  then
11:      Select emigrating island,  $island_k$ , ac-
          cording to  $\mu_i$  using roulette wheel se-
          lection
12:       $island_i(SIV_j) \leftarrow island_k(SIV_j)$ 
13:    end if
14:   end for
15: end for

```

Mutation Operator [36]

```

1: Input: Let population  $P$  has  $n$  islands
   ( $island_i$ ,  $i = 1, 2, \dots, n$ ) and  $m_i$  is the muta-
   tion rate of  $i^{th}$  island.
2: Output: Modified Population  $P$ 
3: for  $i = 1$  to  $n$  do
4:    $m_i = m_{max} * (1 - \frac{P_i}{P_{max}})$ 
5:   if  $m_i > rand$  then
6:     Generate a feasible random value  $R$  in so-
        lution space
7:      $island_i(SIV_j) \leftarrow R$ 
8:   end if
9: end for

```

Improved Biogeography-based Optimization (IBBO)

Improved Migration Operator

```

1: Input: Let  $\lambda_i$  and  $\mu_i$  are the immigration rate and em-
   igration rate of  $i^{th}$  island ( $island_i$ ) respectively.
2: Each island has  $d$  suitability index variables (SIVs) i.e.
   ( $SIV_1$ ,  $SIV_2$  , . . . ,  $SIV_d$ )
3: Let  $P_{modify}$  is the island modification probability.
4: Output: A population of  $m$  modified islands.
5: for  $i = 1$  to Population_Size do
6:   if  $rand < P_{modify}$  then
7:     continue;
8:   end if
9:   for  $j = 1$  to  $d$  do
10:    if  $rand < \lambda_i$  then
11:      Select emigrating island,  $island_k$ , according
        to  $\mu_i$  using roulette wheel selection
12:       $island_i(SIV_j) \leftarrow island_k(SIV_j)$ 
13:    else
14:       $island_i(SIV_j) \leftarrow island_{best}(SIV_j)$ 
15:    end if
16:   end for
17: end for

```

Improved Mutation Operator

```

1: Input: Let population  $P$  has  $n$  islands
   ( $island_i$ ,  $i = 1, 2, \dots, n$ ) and  $m_i$  is the mutation
   rate of  $i^{th}$  island.
2: Output: Modified Population  $P$ 
3: for  $i = 1$  to  $n$  do
4:    $m_i = m_{max} * (1 - \frac{P_i}{P_{max}})$ 
5:   if  $m_i > rand$  then
6:     Randomly generate two permutation ( $P_1^n(i)$ 
   and  $P_2^n(i)$ ) of  $i^{th}$  island
7:      $s_i = P_1^n(i) - P_2^n(i)$ 
8:      $island_i(t + 1) = island_i(t) + s_i * r(t)$ 
9:     Check whether  $island_i(t + 1)$  is feasible or
   not
10:    If not then map to the original bounds
11:   end if
12: end for

```

- IBBO shows limitations for shifted and rotated problems like, CEC 2017 benchmark functions

Spiral Biogeography-based Optimization (SBBO)

- The mutation operator is modified by introducing a **spiral search phase** in mutation along with **random search**
- Spiral Search:**
 - New island are searched in a spiral trajectory defined by Fermat's spiral [69] function

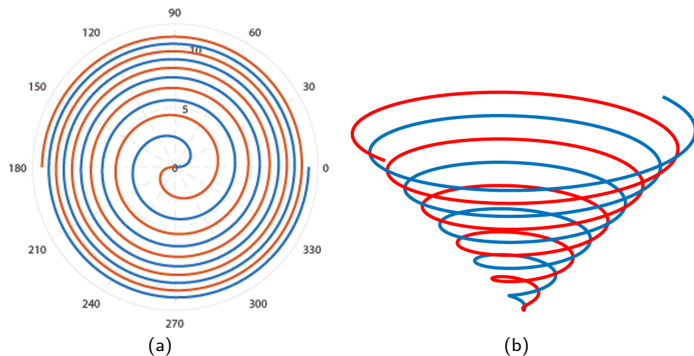


Figure 13: The Fermat's Spiral Function in (a) 2D and (b) 3D



Spiral Biogeography-based Optimization (SBO)

- **Spiral Search:**

- The movement of species in mutation operator is around the best island so far and is defined mathematically by:

$$\text{Island}_i(t+1) = \text{Island}_{\text{Best}}(t) + \text{sgn}(R_i(t)) \cdot |R_i(t)| \cdot l^{1/2} \cdot \cos(2 * \pi * l)$$

where, $R_i(t)$ is the absolute distance between the best island ($\text{Island}_{\text{Best}}$) and i^{th} island at t^{th} iteration as depicted below and l is randomly generated value

$$R_i(t) = \text{Island}_{\text{best}}(t) - \text{Island}_i(t)$$

$$l = 1 + t * \text{random} / \text{max}_{\text{iteration}}$$

- **Random Search:**

- The population diversity in BBO can be increased by random search which generates the new SIVs using the randomly selected islands

$$\text{Island}_i(t+1) = \text{Island}_{\text{random}}(t) - R_i(t)$$

where, $\text{Island}_{\text{random}}(t)$ is any random island at iteration t , $R_i(t)$ is a residual distance from the randomly selected island

$$R_i(t) = \| \text{rand} * \text{Island}_{\text{random}}(t) - \text{Island}_i(t) \|$$

here, $\text{rand} \in (0, 1)$ and Island_i are the i^{th} individual in the population



Spiral Biogeography-based Optimization (SBOO)

Improved Mutation Operator

```
1: Input: Let population  $P$  has  $n$  islands ( $island_i, i = 1, 2, \dots, n$ ) and  $m_i$  is the mutation rate of  $i^{th}$  island
2: Output: Modified Population  $P$ 
3: for  $i = 1$  to  $n$  do
4:   if  $rand \leq 0.5$  then
5:     Update the  $Island_i$  using Spiral search
6:   else
7:     Update the  $Island_i$  using Random search
8:   end if
9: end for
```



Experiment Results

- IBBO and SBBO have been validated against recent meta-heuristic methods
 - Evolutionary-based approaches
 - BBO [61], 2008
 - BBO-M [48], 2014
 - LX-BBO [18], 2016
 - LSHADE [45], 2017
 - Swarm-based approaches
 - GWO [43], 2014
 - ckGSA [44], 2016
 - WOA [42], 2016
 - SSA [41], 2017
- Two sets of benchmarks functions are considered, consisting of both unimodal and multimodal functions
 - Standard Benchmark Functions
 - CEC 2017 Benchmark Problems
- The performance has been evaluated and statistically analyzed in terms of
 - Mean fitness value
 - Friedman test
 - Convergence graph



Experiment Results

Standard benchmark functions

Sr. No.	Function Name	Range	Optimal Value	Optimal Position Values	Category
1.	Ackley	[-35 to 35]	0	(0,...,0)	MM, NS
2.	Alpine	[-10 to 10]	0	(0,...,0)	MM, S
3.	Brown	[-5 to 5]	0	(0,...,0)	UM, NS
4.	Levy	[-10 to 10]	0	(1,1,...,1)	MM
5.	New Schwefel	[-500 to 500]	0	(420.9687,..., 420.9687)	MM
6.	Pathological	[-100 to 100]	0	(0,...,0)	MM, NS
7.	Penalty1	[-50 to 50]	0	(1,1,...,1)	MM, NS
8.	Penalty2	[-50 - 50]	0	(1,1,...,1)	MM, NS
9.	Powell's First Singular	[-4 - 5]	0	(0,0,...,0)	UM, NS
10.	Powell's Second Singular	[-4 - 5]	0	(0,0,...,0)	UM, NS
11.	Powell Sum	[-1 - 1]	0	(0,0,...,0)	UM, S
12.	Quartic	[-1.28 - 1.28]	0	(0,0,...,0)	UM, S
13.	Rastrigin	[-5.12 - 5.12]	0	(0,0,...,0)	MM
14.	Rotated Hyper-Ellipsoid	[-65.536 - 65.536]	0	(0,0,...,0)	UM
15.	Schwefel	[-512 - 512]	-12965.5	(420.9687,..., 420.9687)	MM, S
16.	Schwefel3	[-10 - 10]	0	(0,0,...,0)	MM, NS
17.	Sphere	[-5.12 - 5.12]	0	(0,0,...,0)	UM, S
18.	Step	[-100 - 100]	0	(0,...,0)	UM, S
19.	Sum Squares	[-10 - 10]	0	(0,0,...,0)	UM, S
20.	Trigonometric	[0 - pi]	0	(0,0,...,0)	MM, NS

Experimental Results

- CEC 2017 benchmark functions

S.No.	Function	Optimal Value	Characteristic
1.	Shifted and Rotated Bent Cigar Function	100	
2.	Shifted and Rotated Sum of Different Power Function	200	Unimodal
3.	Shifted and Rotated Zakharov Function	300	
4.	Shifted and Rotated Rosenbrock's Function	400	
5.	Shifted and Rotated Rastrigin's Function	500	
6.	Shifted and Rotated Expanded Scaffer's F6 Function	600	
7.	Shifted and Rotated Lunacek B_Rastrigin Function	700	Simple Multimodal
8.	Shifted and Rotated Non-Continuous Rastrigin's Function	800	
9.	Shifted and Rotated Levy Function	900	
10.	Shifted and Rotated Schwefel's Function	1000	
11.	Hybrid Function 1 (N=3)	1100	
12.	Hybrid Function 2 (N=3)	1200	
13.	Hybrid Function 3 (N=3)	1300	
14.	Hybrid Function 4 (N=4)	1400	
15.	Hybrid Function 5 (N=4)	1500	Hybrid
16.	Hybrid Function 6 (N=4)	1600	
17.	Hybrid Function 6 (N=5)	1700	
18.	Hybrid Function 6 (N=5)	1800	
19.	Hybrid Function 6 (N=5)	1900	
20.	Hybrid Function 6 (N=6)	2000	
21.	Composition Function 1 (N=3)	2100	
22.	Composition Function 2 (N=3)	2200	
23.	Composition Function 3 (N=4)	2300	
24.	Composition Function 4 (N=4)	2400	
25.	Composition Function 5 (N=5)	2500	Composition
26.	Composition Function 6 (N=5)	2600	
27.	Composition Function 7 (N=6)	2700	
28.	Composition Function 8 (N=6)	2800	
29.	Composition Function 9 (N=3)	2900	
30.	Composition Function 10 (N=3)	3000	

Experimental Results- Standard benchmark problems

Func.	Dims.	BBO	BBO-M	GWO	ckGSA	LXBBQ	WOA	LSHADE	SSA	IBBO	SBBO
F1	30	0.1380	1.2600	1.4400	1.2960	0.4710	0.4239	0.1980	0.1782	0.0000	0.0000
	60	0.4960	1.9300	3.1100	2.7990	0.8260	0.7434	0.6340	0.5706	0.0035	0.0024
	90	0.8840	2.4900	3.7800	3.4020	1.0700	0.9630	1.0900	0.9810	0.0863	0.0604
F2	30	0.0005	0.0027	0.8500	0.7650	0.0098	0.0088	0.0005	0.0004	0.0000	0.0000
	60	0.5100	30.4000	31.2000	28.0800	1.8200	1.6380	1.1400	1.0260	0.0000	0.0000
	90	3.8400	84.9000	58.1000	52.2900	5.2600	4.7340	7.4800	6.7320	0.0000	0.0000
F3	30	0.0000	0.0000	0.0000	0.0000	0.0056	0.0051	0.0000	0.0000	0.0000	0.0000
	60	0.0484	0.0015	0.0000	0.0000	4.0500	3.6450	0.1770	0.1593	0.0000	0.0000
	90	1.8800	0.9770	0.0779	0.0701	22.6000	20.3400	4.4900	4.0410	0.0000	0.0000
F4	30	0.0025	0.0000	0.0000	0.0000	0.0080	0.0072	0.0006	0.0005	0.0000	0.0000
	60	0.9950	1.6600	16.0000	14.4000	1.0200	0.9180	1.7100	1.5390	0.0000	0.0000
	90	4.9800	54.3000	59.4000	53.4600	2.7500	2.4750	9.4600	8.5140	0.0000	0.0000
F5	30	12.5	540.0	212.0	190.8	995.0	895.5	17.7	15.9	3.5	2.5
	60	209.0	15000.0	8810.0	7929.0	4550.0	4095.0	551.0	495.9	41.4	29.0
	90	885.0	25400.0	17200.0	15480.0	8730.0	7857.0	2540.0	2286.0	157.0	109.9
F6	30	2.6700	2.9800	4.4100	3.9690	5.0500	4.5450	2.8800	2.5920	2.7600	1.9320
	60	7.5600	6.8600	13.3000	11.9700	12.9000	11.6100	8.5000	7.6500	6.8300	4.7810
	90	14.5000	20.5000	23.4000	21.0600	21.9000	19.7100	17.0000	15.3000	11.2000	7.8400
F7	30	0.0019	0.0000	1.1500	1.0350	0.0233	0.0210	0.0110	0.0099	0.0000	0.0000
	60	8.8	37.0	11.1	10.0	2.8	2.6	15.0	13.5	0.0	0.0
	90	60.7	3710000.0	44.6	40.1	9.2	8.3	3510.0	3159.0	0.1	0.1
F8	30	0.5510	0.0000	2.9200	2.6280	1.6500	1.4850	0.9540	0.8586	0.0000	0.0000
	60	68.5	99.2	146.0	131.4	13.8	12.4	2790.0	2511.0	0.2	0.1
	90	69400.0	8240000.0	1490000.0	1341000.0	44.6	40.1	437000.0	393300.0	1.4	1.0
F9	30	0.7170	21.7000	5.4200	4.8780	0.0840	0.0756	1.3000	1.1700	0.4770	0.3339
	60	43.1	5130.0	59.7	53.7	14.5	13.1	124.0	111.6	5.1	3.6
	90	239.0	17900.0	264.0	237.6	40.9	36.8	461.0	414.9	17.5	12.3
F10	30	0.0084	0.0000	0.0000	0.0000	2.1400	1.9260	0.0003	0.0003	0.0000	0.0000
	60	36.3	4.1	143.0	128.7	71.4	64.3	94.0	84.6	0.0	0.0
	90	597.0	3740.0	10200.0	9180.0	326.0	293.4	1550.0	1395.0	0.0	0.0

First best, Second best, Third best

Experimental Results - Standard benchmark problems

Func.	Dims.	BBO	BBO-M	GWO	ckGSA	LXBBO	WOA	LSHADE	SSA	IBBO	SBBO
F11	30	0.0000	0.0000	0.0000	0.0000	0.0000	0.0000	0.0000	0.0000	0.0000	0.0000
	60	0.0000	0.0000	0.0000	0.0000	0.0000	0.0000	0.0000	0.0000	0.0000	0.0000
	90	0.0000	0.0355	0.0000	0.0000	0.0000	0.0000	0.0000	0.0000	0.0000	0.0000
F12	30	0.0000	0.0000	0.0000	0.0000	0.0000	0.0000	0.0000	0.0000	0.0000	0.0000
	60	0.0005	0.0003	0.0000	0.0000	0.0001	0.0001	0.0006	0.0005	0.0000	0.0000
	90	0.0953	1.5100	0.0000	0.0000	0.0020	0.0018	0.1700	0.1530	0.0000	0.0000
F13	30	0.0000	126.0000	4.5300	4.0770	1.2200	1.0980	0.0000	0.0000	0.0000	0.0000
	60	1.6000	448.0000	75.2000	67.6800	17.5000	15.7500	4.9200	4.4280	0.0000	0.0000
	90	23.0000	833.0000	228.0000	205.2000	54.0000	48.6000	31.3000	28.1700	0.0000	0.0000
F14	30	44.7000	0.0000	1110.0000	999.0000	148.0000	133.2000	91.8000	82.6200	0.6300	0.4410
	60	3210.0000	10.6000	64600.0000	58140.0000	2250.0000	2025.0000	6810.0000	6129.0000	67.1000	46.9700
	90	28000.0000	9340.0000	323000.0000	290700.0000	8850.0000	7965.0000	54400.0000	48960.0000	742.0000	519.4000
F15	30	120.0000	1760.0000	554.0000	498.6000	92.5000	83.2500	22.1000	19.8900	5.0900	3.5630
	60	210.0000	8050.0000	3960.0000	3564.0000	4160.0000	3744.0000	511.0000	459.9000	30.5000	21.3500
	90	1180.0000	17300.0000	7740.0000	6966.0000	9430.0000	8487.0000	2420.0000	2178.0000	141.0000	98.7000
F16	30	0.0000	0.0000	21.1000	18.9900	0.0744	0.0670	0.0053	0.0048	0.0000	0.0000
	60	2.0000	0.7310	99.4000	89.4600	5.4600	4.9140	4.0700	3.6630	0.0000	0.0000
	90	10.8000	30.0000	222.0000	199.8000	14.6000	13.1400	19.8000	17.8200	0.0000	0.0000
F17	30	0.0010	0.0000	1.8200	1.6380	1.5100	1.3590	0.1400	0.1260	0.0000	0.0000
	60	0.1930	0.0033	21.8000	19.6200	0.2490	0.2241	0.7730	0.6957	0.0000	0.0000
	90	2.9600	2.0600	76.0000	68.4000	1.0600	0.9540	7.7700	6.9930	0.0000	0.0000
F18	30	0.3000	0.0000	113.0000	101.7000	1.9000	1.7100	2.4000	2.1600	0.2000	0.1400
	60	28.7000	0.0000	510.0000	459.0000	42.5000	38.2500	57.8000	52.0200	6.7000	4.6900
	90	128.0000	101.0000	1050.0000	945.0000	106.0000	95.4000	256.0000	230.4000	23.4000	16.3800
F19	30	0.0096	0.0000	1.8200	1.6380	1.5100	1.3590	0.1400	0.1260	0.0000	0.0000
	60	51.2000	0.2360	676.0000	608.4000	41.6000	37.4400	142.0000	127.8000	0.0000	0.0000
	90	665.0000	204.0000	4510.0000	4059.0000	190.0000	171.0000	1420.0000	1278.0000	0.0000	0.0000
F20	30	2.4300	0.0009	30.1000	27.0900	14.7000	13.2300	2.3500	2.1150	0.0000	0.0000
	60	176.0000	0.3300	4.1700	3.7530	1700.0000	1530.0000	315.0000	283.5000	0.0000	0.0000
	90	1300.0000	12.9000	21.6000	19.4400	6230.0000	5607.0000	1880.0000	1692.0000	0.0000	0.0000

First best, Second best, Third best

Experimental Results- CEC benchmark problems

Func.	BBO	BBO-M	LX-BBO	IBBO	ckGSA	SSA	LSHADE	GWO	WOA	SBBO
F1	6.20E+09	6.51E+09	8.96E+06	7.82E+10	2.05E+10	2.15E+10	1.41E+11	4.88E+09	6.32E+08	1.61E+07
F3	1.38E+05	1.01E+05	1.63E+05	4.62E+05	1.81E+05	1.82E+05	4.74E+05	8.61E+04	1.77E+05	3.94E+04
F4	1.20E+03	1.26E+03	6.52E+02	1.68E+04	4.18E+03	4.38E+03	1.78E+04	8.63E+02	9.74E+02	5.05E+02
F5	8.20E+02	8.45E+02	7.36E+02	1.15E+03	8.39E+02	8.38E+02	1.40E+03	6.97E+02	9.57E+02	5.77E+02
F6	6.13E+02	6.20E+02	6.12E+02	6.69E+02	6.65E+02	6.65E+02	6.79E+02	6.12E+02	6.82E+02	6.00E+02
F7	1.33E+03	1.30E+03	1.37E+03	2.76E+03	1.37E+03	1.38E+03	5.85E+03	1.04E+03	1.73E+03	8.21E+02
F8	1.14E+03	1.13E+03	1.03E+03	1.45E+03	1.16E+03	1.16E+03	1.67E+03	1.00E+03	1.26E+03	8.82E+02
F9	4.86E+03	5.17E+03	7.34E+03	3.50E+04	1.20E+04	1.20E+04	6.08E+04	5.69E+03	2.71E+04	1.78E+03
F10	9.94E+03	1.03E+04	6.85E+03	1.36E+04	8.42E+03	8.56E+03	1.28E+04	7.39E+03	1.10E+04	4.56E+03
F11	3.50E+03	2.52E+03	1.70E+03	4.51E+04	1.95E+04	1.99E+04	3.00E+04	3.28E+03	2.24E+03	1.73E+03
F12	2.86E+08	3.19E+08	2.11E+07	2.27E+10	5.30E+09	6.24E+09	1.91E+10	4.68E+08	5.57E+08	1.97E+06
F13	7.73E+05	6.69E+05	1.76E+05	9.93E+09	3.75E+07	9.57E+07	3.23E+09	1.63E+08	6.57E+06	9.71E+07
F14	1.91E+06	8.03E+05	9.17E+05	3.78E+07	7.11E+06	5.54E+06	7.88E+06	7.42E+05	2.47E+06	2.36E+05
F15	8.03E+04	1.47E+04	2.24E+04	3.50E+09	1.89E+07	5.83E+07	8.02E+08	1.33E+07	6.26E+05	2.42E+04

First best, Second best, Third best



Experimental Results- CEC benchmark problems

Func.	BBO	BBO-M	LX-BBO	IBBO	ckGSA	SSA	LSHADE	GWO	WOA	SBBO
F16	3.44E+03	3.38E+03	3.57E+03	6.60E+03	4.70E+03	4.57E+03	6.21E+03	2.91E+03	5.48E+03	2.81E+03
F17	2.92E+03	2.95E+03	3.24E+03	1.15E+04	3.80E+03	3.76E+03	7.42E+03	2.79E+03	4.25E+03	2.24E+03
F18	6.35E+06	3.71E+06	6.31E+06	1.60E+08	5.94E+06	8.40E+06	4.59E+07	3.78E+06	1.79E+07	1.54E+06
F19	6.53E+04	1.73E+04	2.65E+04	1.18E+09	2.89E+05	3.44E+05	2.43E+08	4.85E+06	6.55E+06	1.94E+04
F20	3.08E+03	2.88E+03	3.41E+03	4.58E+03	3.74E+03	3.67E+03	3.91E+03	2.84E+03	3.71E+03	2.61E+03
F21	2.63E+03	2.63E+03	2.55E+03	2.95E+03	2.87E+03	2.87E+03	3.08E+03	2.49E+03	2.95E+03	2.39E+03
F22	1.22E+04	1.08E+04	8.69E+03	1.53E+04	1.21E+04	1.22E+04	1.47E+04	8.88E+03	1.25E+04	4.66E+03
F23	3.09E+03	3.12E+03	3.03E+03	3.61E+03	4.89E+03	4.82E+03	3.36E+03	2.93E+03	3.63E+03	2.79E+03
F24	3.30E+03	3.34E+03	3.21E+03	3.79E+03	4.59E+03	4.64E+03	3.48E+03	3.13E+03	3.70E+03	3.00E+03
F25	3.53E+03	3.60E+03	3.12E+03	1.42E+04	4.78E+03	4.91E+03	3.38E+04	3.42E+03	3.39E+03	2.89E+03
F26	7.49E+03	7.90E+03	6.85E+03	1.30E+04	1.24E+04	1.27E+04	9.96E+03	6.00E+03	1.34E+04	5.00E+03
F27	3.56E+03	3.61E+03	3.27E+03	4.81E+03	8.07E+03	8.35E+03	3.60E+03	3.55E+03	4.42E+03	3.26E+03
F28	3.82E+03	3.91E+03	3.48E+03	1.06E+04	5.94E+03	6.07E+03	8.39E+03	3.92E+03	4.04E+03	3.38E+03
F29	4.28E+03	4.35E+03	4.37E+03	1.05E+04	1.18E+04	1.19E+04	6.32E+03	4.41E+03	7.91E+03	3.93E+03

First best, Second best, Third best



Experimental Results

Table 7: Mean ranking of considered algorithms using Friedman Test

Rank	Algorithm	Mean Rank Value
1	SBBO	1.93
2	BBO-M	3.70
3	GWO	3.93
4	LX-BBO	4.70
5	BBO	4.12
6	cKGSA	6.97
7	WOA	6.97
8	SSA	7.92
9	LSHADE	8.57
10	IBBO	9.52



Experimental Results

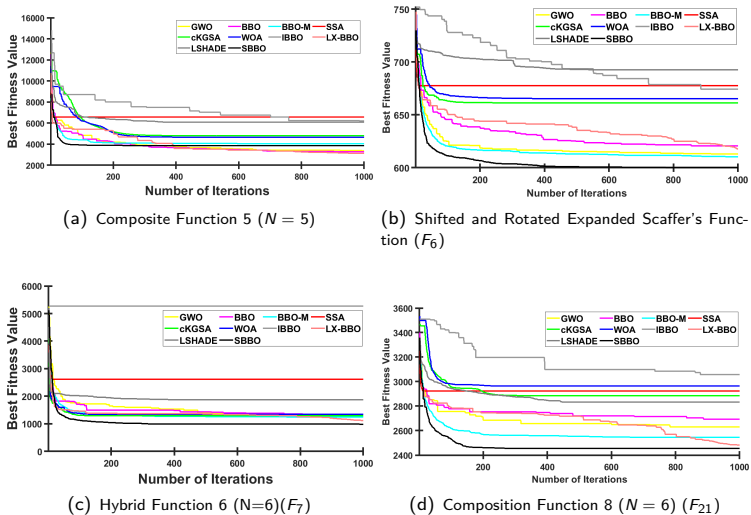
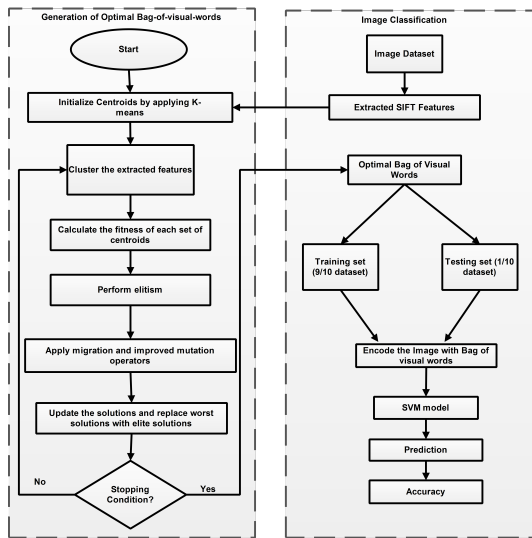


Figure 14: Convergence trend of SBBO with other considered Meta-heuristics.

Codebook Generation using SBBO



- Let F is a set of local features $\{f_1, f_2, \dots, f_N\}$, where $f_n \in \mathbb{R}^D$
- Apply K-means clustering on the set F to find the initial K cluster centers $\{c_1, c_2, \dots, c_K\}$ where $c_k \in \mathbb{R}^D$.
- Objective function:**

$$\text{Min. } \delta(f_m, c_k) = \sum_{i=1}^N \sum_{j=1}^K \| f_m - c_k \|^2$$

Figure 15: The flow chart of proposed method

Experiment Results - Confusion matrix - Blue Histology Dataset

BOF		Predicted			
Actual		CT	ET	MT	NT
	CT	0.75	0.1	0.15	0
	ET	0.45	0.35	0.2	0
	MT	0.2	0.05	0.75	0
	NT	0.6	0.15	0.2	0.05

(a) BOF

IB3		Predicted			
Actual		CT	ET	MT	NT
	CT	0.35	0.2	0.3	0.15
	ET	0.04	0.6	0.2	0.16
	MT	0.35	0.1	0.3	0.25
	NT	0.35	0.25	0.05	0.35

(b) IB3

IKS2		Predicted			
Actual		CT	ET	MT	NT
	CT	0.85	0.05	0.1	0
	ET	0.36	0.35	0.2	0.04
	MT	0.15	0.05	0.75	0.05
	NT	0.6	0.15	0.2	0.05

(c) IKS2

BBO-BOF		Predicted			
Actual		CT	ET	MT	NT
	CT	0.85	0.05	0.08	0.02
	ET	0.06	0.65	0.16	0.08
	MT	0.05	0.1	0.75	0.1
	NT	0.45	0.15	0.2	0.2

(d) BBO-BOF

SBBO-BOF		Predicted			
Actual		CT	ET	MT	NT
	CT	0.69	0.12	0.09	0.09
	ET	0.03	0.9	0	0.07
	MT	0	0.19	0.81	0
	NT	0.161	0.29	0.07	0.49

(e) SBBO-BOF

Figure 16: The normalized confusion matrix for the blue histology tissue dataset for the five methods (a) BOF, (b) IKS2, (c) BBO-BOF, and (d) SBBO-BOF

Experiment Results - Confusion matrix - ADL Dataset

Table 8: The confusion matrix for kidney image classification

Class	Healthy	Inflammatory	Method
Healthy	0.6925	0.3075	SVM
	0.875	0.125	SRC
	0.825	0.175	SHIRC
	0.89	0.11	SBBO-BOF
Inflammatory	0.2812	0.7188	SVM
	0.25	0.75	SRC
	0.1667	0.8333	SHIRC
	0.175	0.875	SBBO-BOF

Table 9: The confusion matrix for lung image classification

Class	Healthy	Inflammatory	Method
Healthy	0.8875	0.1125	SVM
	0.725	0.275	SRC
	0.75	0.25	SHIRC
	0.92	0.08	SBBO-BOF
Inflammatory	0.372	0.6238	SVM
	0.2417	0.7853	SRC
	0.15	0.85	SHIRC
	0.15	0.85	SBBO-BOF

Table 10: The confusion matrix for spleen image classification

Class	Healthy	Inflammatory	Method
Healthy	0.5112	0.488	SVM
	0.7083	0.2917	SRC
	0.65	0.35	SHIRC
	0.828	0.172	SBBO-BOF
Inflammatory	0.1275	0.8725	SVM
	0.2083	0.7917	SRC
	0.1167	0.8833	SHIRC
	0.1	0.9	SBBO-BOF



Experiment Results

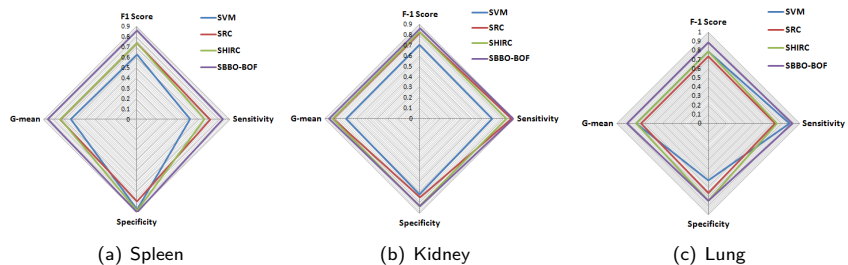


Figure 17: Radar chart for average results on (a) Spleen dataset, (b) Kidney dataset, and (c) Lung dataset.

Table 11: Comparative analysis of the proposed meta-heuristic based classification method.

Dataset	BOF	IKS2	BBO-BOF	IBBO-BOF	SBBO-BOF
Blue Histology	47.5	50.63	62.03	65	72.23
ADL	70.6	72.5	78.5	69.1	87

Research contribution

- An efficient spiral biogeography-based optimization (SBBO) based on Fermat's spiral has been presented which shows better convergence precision on both the standard benchmark functions and CEC 2017 functions
- The SBBO is used to enhance the codebook generation method in BOF framework
- The proposed BOF method gives the accuracy 72.23% and 87% for Blue histology and ADL dataset respectively



Objectives

- ① To design a new keypoint selection method for finding discriminative and relevant features for codebook construction
- ② To design an efficient meta-heuristic based codebook generation method to reduce the effect of dense regions of histopathological images
- ③ To design a computationally efficient and effective codebook generation method for finding the relevant visual words
- ④ To design an efficient feature encoding method by incorporating the merits of two different features descriptors for the better image representation



Grey Relational Analysis based Bag-of-Features (GRA-BOF)

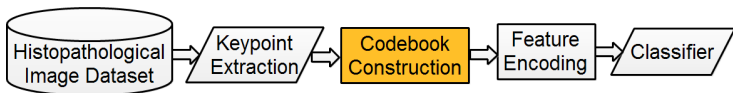


Figure 18: Flow chart of the BOF method

- GRA based feature selection method produce significant features due to effective GRG similarity measure and is computationally efficient.
- However, due to the use of K-means, feature selection based BOF method produces less accuracy
- In the second approach, meta-heuristic based method performs better, however they are computationally expensive
- Therefore, in this work GRA has been used as a clustering method for obtaining optimal visual words in better computational cost



Keypoint Clustering using GRA

The GRA-BOF Method

-
- 1: **Input:** A set of feature vectors known as descriptor D having n strong feature vectors and a cut-off threshold (T)
 - 2: **Output:** Reduced descriptor S having m feature vectors ($m < n$)
 - 3: **while** ($\text{size}(D) > 1$) **do**
 - 4: Select a reference vector (R) near to the mean of D
 - 5: $D = D - R$
 - 6: Calculate GRGs (Γ) for each feature vector in D with R

$$\Gamma(R, d) = \frac{1}{D} \sum_{d=1}^D [\gamma(R, d)]$$

where,

$$\gamma(R, d) = \frac{\min \Delta(d) + \xi \max \Delta(d)}{\Delta(d) + \xi \max \Delta(d)},$$

where, $\Delta(d) = |R(d) - D(d)|$ and $\xi \in (0, 1]$.

- 7: Delete the $T\%$ feature vectors, having the highest GRG values, from D
 - 8: Update vector $S = [S \ R]$
 - 9: **end while**
 - 10: Use S to generate histograms.
 - 11: Train SVM classifier for classification of images into their respective categories.
-

Keypoint Clustering using GRA

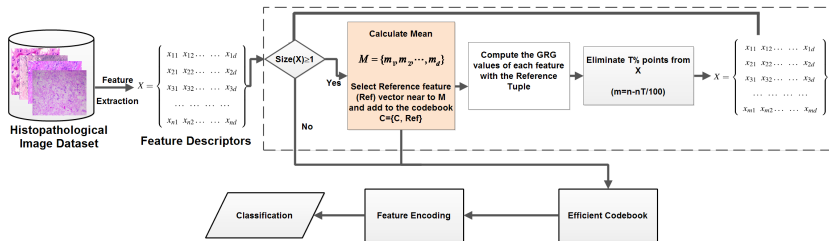


Figure 19: The GRA based BOF method

Selection of cut-off threshold (T) value for GRA-BOF

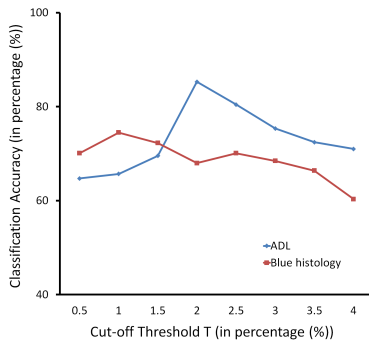


Figure 20: Impact analysis of cut-off threshold (T) value over classification accuracy on ADL and Blue histology datasets.

Classification Performance

Table 12: Classification performance with other methods based on recall, precision, F1 score, specificity, and average accuracy on ADL three organs dataset.

Organ	Algorithms	Recall	Specificity	Precision	FPR	Accuracy
Kidney	SVM	0.69	0.72	0.71	0.28	0.71
	SRC	0.88	0.75	0.78	0.25	0.81
	SHIRC	0.83	0.83	0.83	0.17	0.83
	BOF	0.82	0.69	0.73	0.31	0.76
	IKS2-BOF	0.85	0.77	0.79	0.23	0.81
	GRA-BOF	0.89	0.91	0.91	0.09	0.90
Lung	SVM	0.89	0.63	0.70	0.37	0.76
	SRC	0.73	0.76	0.75	0.24	0.75
	SHIRC	0.75	0.85	0.83	0.15	0.80
	BOF	0.72	0.75	0.74	0.25	0.74
	IKS2-BOF	0.83	0.70	0.73	0.30	0.77
	GRA-BOF	0.92	0.94	0.94	0.06	0.93
Spleen	SVM	0.51	0.87	0.80	0.13	0.69
	SRC	0.71	0.79	0.77	0.21	0.75
	SHIRC	0.65	0.88	0.85	0.12	0.77
	BOF	0.55	0.77	0.71	0.23	0.66
	IKS2-BOF	0.68	0.87	0.84	0.13	0.78
	GRA-BOF	0.75	0.89	0.87	0.11	0.82

Classification Performance

Table 13: Classification performance with other methods based on recall, precision, F1 score, specificity, and average accuracy on Blue histology dataset

Category	Parameters	SVM	SRC	SHIRC	BOF	IKS2	GRA-BOF
CT	Recall	0.450	0.650	0.550	0.750	0.710	0.800
	Precision	0.512	0.512	0.500	0.375	0.399	0.696
	F1 Score	0.573	0.573	0.524	0.500	0.511	0.744
	Specificity	0.806	0.806	0.814	0.583	0.643	0.883
ET	Recall	0.400	0.583	0.700	0.350	0.330	0.780
	Precision	0.778	0.778	0.778	0.538	0.524	0.650
	F1 Score	0.667	0.667	0.737	0.424	0.405	0.709
	Specificity	0.933	0.933	0.932	0.900	0.900	0.860
MT	Recall	0.300	0.750	0.737	0.750	0.730	0.751
	Precision	0.652	0.652	0.700	0.577	0.570	0.815
	F1 Score	0.698	0.698	0.718	0.652	0.640	0.781
	Specificity	0.875	0.875	0.900	0.817	0.817	0.943
NT	Recall	0.200	0.480	0.550	0.050	0.250	0.650
	Precision	0.545	0.545	0.579	1.000	0.806	0.890
	F1 Score	0.511	0.511	0.564	0.095	0.382	0.751
	Specificity	0.875	0.875	0.864	1.000	0.980	0.973
	Average Accuracy	33.8	61.4	63.3	47.5	50.5	74.5

Classification Performance

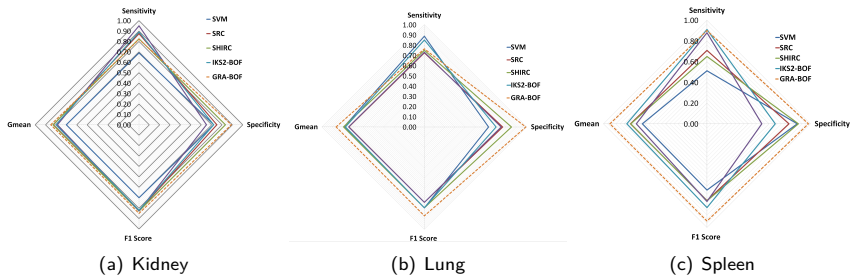


Figure 21: Radar Charts for average results obtained for SVM classifier on a) ADL dataset and b) Tissue image dataset by considering F-1 score, sensitivity, specificity, and G-mean

Table 14: Comparative analysis of the proposed GKS based BOF method with other considered methods in terms of average accuracy. The best results are in bold

Category	SVM	SRC	SHIRC	BOF	IKS2	GRA-BOF
ADL Dataset	72	77	80	72	69	88.3
Blue Histology	29	33	50	30	43	74.5



Research Contribution

- A new Grey relational analysis based BOF method (GRA-BOF) which improves the efficiency of vector quantization step of the standard BOF method is introduced
- The GRA-BOF method has been validated on two datasets, Blue histology and ADL histopathological image dataset
- The average accuracy of the GRA-BOF method is 88.3% which is the highest among other state-of-the-art methods followed by SRC (81.9%) and SHIRC (78.9%)
- The experimental results validate that the GRA-BOF method outperforms the other considered methods for histopathological image classification



Objectives

- ① To design a new keypoint selection method for finding discriminative and relevant features for codebook construction
- ② To design an efficient meta-heuristic based codebook generation method to reduce the effect of dense regions of histopathological images
- ③ To design a computationally efficient and effective codebook generation method for finding the relevant visual words
- ④ To design an efficient feature encoding method by incorporating the merits of two different features descriptors for the better image representation



Weighted Two Dimensional Vector Quantization

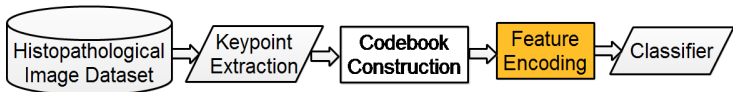


Figure 22: Flow chart of the BOF method

- Single feature based vector quantization method represents the images into histograms, however, every feature extraction method produces different feature vector with various qualities and shortcomings
- Such as, SIFT produces better results than SURF when applied on images having different scales [53]
- SURF works well for noisy and blurred images [53]
- ORB performs better in rotation and noise than SIFT [26]
- That's why, this work introduces a weighted two dimensional vector quantization method based on the information of two different feature descriptors



Weighted Two Dimensional Vector Quantization

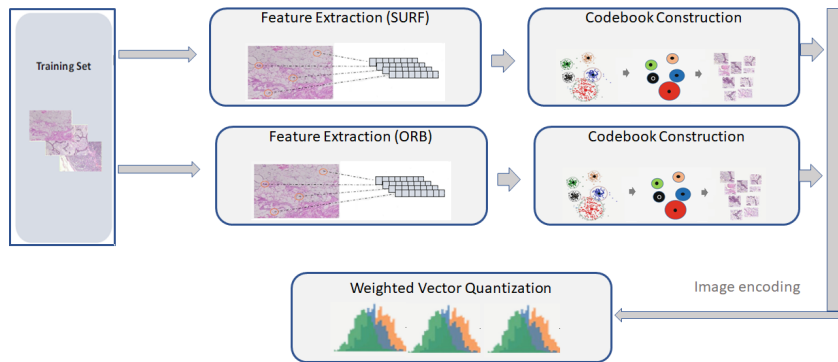


Figure 23: Flow chart of weighted two dimensional vector quantization



Weighted Two Dimensional Vector Quantization

- Let $X = [x_1, x_2, \dots, x_N] \in \mathbb{R}^{D \times N}$ be N D -dimensional features extracted from an image and $\mathcal{B}_i = [b_1, b_2, \dots, b_K] \in \mathbb{R}^{D \times N}$ is a codebook of K codewords. The objective of encoding is to compute a code s for input x with D
- In current voting based methods, each descriptor x is represented by a code $s(i) = \phi(x)$, $i = 1, 2, \dots, K$ which is determined by its voting value to codeword d

$$\phi(x) = \begin{cases} 1 & \text{if } i = \operatorname{argmin}_j (\|x - b_j\|_2) \\ 0 & \text{otherwise} \end{cases}$$

- Let $Y = [y_1, y_2, \dots, y_N] \in \mathbb{R}^{D \times N}$ be the another N D -dimensional features extracted from an image and $\mathcal{C}_i = [c_1, c_2, \dots, c_K] \in \mathbb{R}^{D \times N}$ be the codebook with K codewords then the weighted two dimensional vector quantization is defined as follows:

$$\forall_i s(i, j) = \alpha \cdot \phi_1(x) + (1 - \alpha) \cdot \phi_2(x), \quad j = 1, 2, \dots, K$$

where, α is a weighting factor between zero and one



Experimental Analysis

Table 15: Comparative analysis of considered methods on ADL dataset in terms of various performance parameters

Organ	Algorithms	Sensitivity	Specificity	Precision	FNR	Accuracy
Kidney	SIFT	0.670	0.720	0.705	0.330	0.695
	ORB	0.650	0.710	0.691	0.350	0.680
	SURF	0.640	0.700	0.681	0.360	0.670
	SIFT+ORB	0.780	0.828	0.821	0.220	0.804
	SIFT+SURF	0.844	0.490	0.598	0.156	0.658
	ORB+SURF	0.690	0.830	0.802	0.310	0.760
Lung	SIFT	0.740	0.730	0.733	0.260	0.735
	ORB	0.730	0.720	0.723	0.270	0.725
	SURF	0.720	0.710	0.713	0.280	0.715
	SIFT+ORB	0.820	0.830	0.828	0.180	0.825
	SIFT+SURF	0.790	0.810	0.806	0.210	0.800
	ORB+SURF	0.790	0.740	0.752	0.210	0.765
Spleen	SIFT	0.590	0.750	0.702	0.410	0.670
	ORB	0.580	0.760	0.707	0.420	0.670
	SURF	0.570	0.750	0.695	0.430	0.660
	SIFT+ORB	0.760	0.790	0.784	0.240	0.775
	SIFT+SURF	0.720	0.780	0.766	0.280	0.750
	ORB+SURF	0.670	0.780	0.753	0.330	0.725

Experimental Analysis

Table 16: Comparative analysis of the considered methods on Blue Histology dataset in terms of various performance parameters

Category	Algorithms	Sensitivity	Specificity	Precision	FNR	F1 Score
CT	SIFT	0.84	0.75	0.54	0.16	0.66
	ORB	0.80	0.68	0.46	0.20	0.58
	SURF	0.70	0.75	0.48	0.30	0.57
	SIFT+ORB	0.86	0.95	0.85	0.14	0.85
	SIFT+SURF	0.70	0.83	0.58	0.30	0.64
	ORB+SURF	0.70	0.91	0.73	0.30	0.71
ET	SIFT	0.64	0.84	0.58	0.36	0.61
	ORB	0.53	0.90	0.63	0.47	0.57
	SURF	0.63	0.87	0.60	0.37	0.62
	SIFT+ORB	0.76	0.94	0.80	0.24	0.78
	SIFT+SURF	0.75	0.90	0.71	0.25	0.73
	ORB+SURF	0.69	0.88	0.66	0.31	0.68
MT	SIFT	0.55	0.95	0.79	0.45	0.65
	ORB	0.75	0.85	0.63	0.25	0.68
	SURF	0.65	0.92	0.72	0.35	0.68
	SIFT+ORB	0.78	0.91	0.74	0.22	0.76
	SIFT+SURF	0.60	0.90	0.67	0.40	0.63
	ORB+SURF	0.70	0.97	0.88	0.30	0.78
NT	SIFT	0.31	0.93	0.56	0.69	0.40
	ORB	0.05	0.95	0.25	0.95	0.08
	SURF	0.35	0.92	0.58	0.65	0.44
	SIFT+ORB	0.69	0.90	0.72	0.31	0.70
	SIFT+SURF	0.60	0.92	0.71	0.40	0.65
	ORB+SURF	0.65	0.82	0.54	0.35	0.59

Classification Accuracy

Table 17: Comparative analysis of the proposed 2DVQ method average classification accuracy

Features	Encoding	ADL	Blue histology
SIFT	HV	70	62
ORB	HV	69	53
SURF	HV	68	58
SIFT+ORB	2DVQ	79	74
SIFT+SURF	2DVQ	74	66
ORB+SURF	2DVQ	75	69



Research Contribution

- In this work, a weighted two dimensional vector quantization method has been introduced
- The proposed method measures the weighted information of two different feature descriptors, namely SIFT and ORB

Efficient Bag-of-Features Method for Histopathological Image Classification

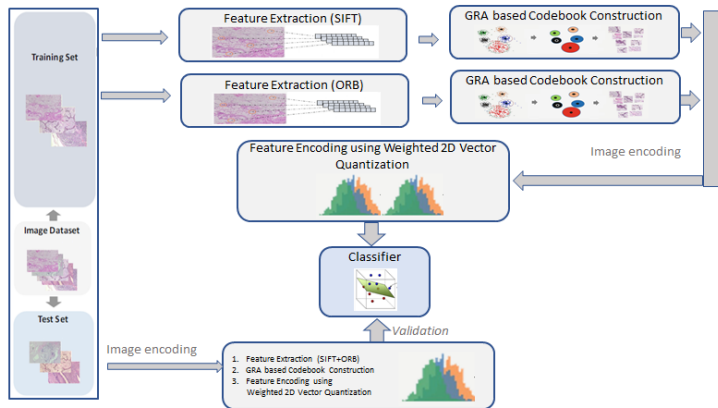


Figure 24: The proposed Bag-of-feature approach for Histopathological image classification [9]

Efficient Bag-of-Features Method for Histopathological Image Classification

Table 18: The performance comparison of various proposed BOF methods on ADL and Blue histology dataset.

S.No.	BOF Approach	ADL	Blue Histology
		Dataset	Dataset
1.	GKS-BOF	78	48
2.	SBBO-BOF	87	72.23
3.	GRA-BOF	88.3	74.5
4.	Weighted-BOF	79	74
5.	GRA-Weighted-BOF	91.2	77.5
6.	Bayramoglu et al. [6]	52.72	28.12
7.	CNN-IBBO-BOF [52]	87.66	67



Conclusion I

- A new Grey relational analysis based keypoints selection phase has been introduced in BOF method which reduces the extracted high dimensional features by 95% and 68% from the ADL and Blue histology datasets respectively. This also increases the respected classification accuracy by 13% and 11%.
- To overcome the limitations of k-means based codebook construction algorithm in BOF method, an optimal SBBO has been presented which gives the best mean ranking of 1.93 by Friedman test. It produces 72.23% and 87% accuracy for Blue histology and ADL datasets respectively. However, the method is computationally expensive.
- To make the codebook construction computationally efficient, a new GRA-BOF has been presented which improves the efficiency of codebook construction step of the standard BOF method and gives the accuracy of 74.5% and 88.3% for Blue histology and ADL datasets respectively.



Conclusion II

- To take the merits of two different feature descriptors, a new weighted two dimensional vector quantization method has been introduced which gives the classification accuracy 74% and 79% for Blue histology and ADL datasets respectively using SIFT and ORB features.
- Finally, a new and efficient bag-of-features model is presented using GRA based code-book construction and weighted 2D vector quantization methods. The presented model gives the classification accuracy 77.5% and 91.2% for Blue histology and ADL datasets respectively which is the best among other methods.



Future Work

- The developed BOF method can be used to analyze the different structures of histopathological and cytological images.
- The proposed keypoints selection method may be applied to other data sets such as microarrays data sets.
- The developed classification system may be explored for solving other real world pattern recognition problems.
- The classification of the accuracy of the system can be increased by introducing some pre-processing steps in tissue images.



Research Papers

International Journals

- R. Pal and M. Saraswat, "Improved Biogeography based optimization", *International Journal of Advanced Intelligence Paradigms*, 2017. (In press) (Indexing: Scopus, H-index: 7)
- R. Pal and M. Saraswat, "Grey Relational Analysis based Keypoint selection in Bag-of-Features for Histopathological Image Classification", *Recent Patents on Computer Science*, 2018. (In Press) (Indexing: Scopus, H-index: 9)
- R. Pal and M. Saraswat, "Histopathological Image Classification using Enhanced Bag-of-Feature with Spiral Biogeography-based Optimization", *Applied Intelligence, Springer*, Volume 49, Issue 9, pp 3406–3424, 2019. (Indexing: SCI, H-index: 36)
- R. Pal and M. Saraswat, "A New Weighted Two Dimensional Vector Quantization Encoding Method in Bag-of-Features for Histopathological Image Classification", *International Journal of Intelligent Information and Database Systems*, 2019. (In press)(Indexing: Scopus, H-index: 10)
- R. Pal and M. Saraswat, "Efficient Bag-Of-Features using grey relational analysis for Histopathology Image classification", *Computers in Biology and Medicine*. (Under review)

International Conferences

- R. Pal and M. Saraswat, "Data clustering using enhanced Biogeography based optimization", In proc. of *Tenth International Conference on Contemporary Computing (IC3)*, pp. 1-6, 2017.
- R. Pal and M. Saraswat, "Enhanced Bag of Features using AlexNet and improved biogeography-based optimization for Histopathological Image Analysis", *Eleventh International Conference on Contemporary Computing (IC3)*, pp. 1-6, 2018.
- R. Pal and M. Saraswat, "A new Bag-of-feature method using Biogeography-based Optimization for categorization of Histology images", The 4th International Conference on Computers and Management, Delhi, India, pp. 155-160, 2018.

Acknowledgment

I am thankful to Science and Engineering Research Board, Department of Science & Technology, Government of India, New Delhi for funding this work as part of the project (ECR/2016/000844).



Key References I

- [1] Histopathological image data sets.

<http://signal.ee.psu.edu/histimg2.html>.

(Accessed on 08/04/2018).

- [2] Shivani Agarwal, Aatif Awan, and Dan Roth.

Learning to detect objects in images via a sparse, part-based representation.

IEEE transactions on pattern analysis and machine intelligence, 26(11):1475–1490, 2004.

- [3] David W Aha, Dennis Kibler, and Marc K Albert.

Instance-based learning algorithms.

Machine Learning, 6:37–66, 1991.

- [4] Yaniv Bar, Idit Diamant, Lior Wolf, Sivan Lieberman, Eli Konen, and Hayit Greenspan.

Chest pathology detection using deep learning with non-medical training.

In *ISBI*, pages 294–297. Citeseer, 2015.

- [5] Herbert Bay, Andreas Ess, Tinne Tuytelaars, and Luc Van Gool.

Speeded-up robust features (surf).

Computer vision and image understanding, 110(3):346–359, 2008.

- [6] Neslihan Bayramoglu, Juho Kannala, and Janne Heikkilä.

Deep learning for magnification independent breast cancer histopathology image classification.

In *Proc. of International conference on pattern recognition, Cancun, Mexico*, pp. 2440–2445, 2016.

- [7] Dragan Bošnački, Natal van Riel, and Mitko Veta.

Deep learning with convolutional neural networks for histopathology image analysis.

In *Automated Reasoning for Systems Biology and Medicine*, pages 453–469. Springer, 2019.

Key References II

- [8] Henry Brighton and Chris Mellish.
Advances in instance selection for instance-based learning algorithms.
Data Mining and Knowledge Discovery, 6:153–172, 2002.
- [9] Juan C Caicedo, Angel Cruz, and Fabio A Gonzalez.
Histopathology image classification using bag of features and kernel functions.
In *Conference on Artificial Intelligence in Medicine in Europe*, pages 126–135. Springer, 2009.
- [10] Hang Chang, Nandita Nayak, Paul T Spellman, and Bahram Parvin.
Characterization of tissue histopathology via predictive sparse decomposition and spatial pyramid matching.
In *International Conference on Medical Image Computing and Computer-Assisted Intervention*, pages 91–98. Springer, 2013.
- [11] KC Chang, RG Lee, C Wen, and MF Yeh.
Comparison of similarity measures for clustering electrocardiogram complexes.
In *Computers in Cardiology*, 2005, pages 759–762. IEEE, 2005.
- [12] Dan C Cireşan, Alessandro Giusti, Luca M Gambardella, and Jürgen Schmidhuber.
Mitosis detection in breast cancer histology images with deep neural networks.
In *International Conference on Medical Image Computing and Computer-assisted Intervention*, pages 411–418. Springer, 2013.
- [13] Angel Cruz-Roa, Juan C Caicedo, and Fabio A González.
Visual pattern mining in histology image collections using bag of features.
Artificial intelligence in medicine, 52(2):91–106, 2011.
- [14] Angel Alfonso Cruz-Roa, John Edison Arevalo Ovalle, Anant Madabhushi, and Fabio Augusto González Osorio.
A deep learning architecture for image representation, visual interpretability and automated basal-cell carcinoma cancer detection.
In *International Conference on Medical Image Computing and Computer-Assisted Intervention*, pages 403–410. Springer, 2013.



Key References III

- [15] Matthew D DiFranco, Gillian O Hurley, Elaine W Kay, R William G Watson, and Padraig Cunningham.
Ensemble based system for whole-slide prostate cancer probability mapping using color texture features.
Computerized medical imaging and graphics, 35(7):629–645, 2011.
- [16] Jérôme Fournier, Matthieu Cord, and Sylvie Philipp-Foliguet.
Retin: A content-based image indexing and retrieval system.
Pattern Analysis & Applications, 4(2-3):153–173, 2001.
- [17] Joseph Galaro, Alexander R Judkins, David Ellison, Jennifer Baccon, and Anant Madabhushi.
An integrated texton and bag of words classifier for identifying anaplastic medulloblastomas.
In *Engineering in Medicine and Biology Society, EMBC, 2011 Annual International Conference of the IEEE*, pages 3443–3446. IEEE, 2011.
- [18] Vanita Garg and Kusum Deep.
Performance of laplacian biogeography-based optimization algorithm on cec 2014 continuous optimization benchmarks and camera calibration problem.
Swarm and Evolutionary Computation, 27:132–144, 2016.
- [19] Bogdan Georgescu, Ilan Shimshoni, and Peter Meer.
Mean shift based clustering in high dimensions: A texture classification example.
In *ICCV*, volume 3, page 456, 2003.
- [20] Madhumala Ghosh, Devkumar Das, Subhodip Mandal, Chandan Chakraborty, Mallika Pala, Ashok K Maity, Surjya K Pal, and Ajoy K Ray.
Statistical pattern analysis of white blood cell nuclei morphometry.
In *Students' Technology Symposium (TechSym), 2010 IEEE*, pages 59–66. IEEE, 2010.
- [21] Metin N Gurcan, Laura E Boucheron, Ali Can, Anant Madabhushi, Nasir M Rajpoot, and Bulent Yener.
Histopathological image analysis: A review.
IEEE reviews in biomedical engineering, 2:147–171, 2009.



Key References IV

- [22] Ricardo Gutiérrez, Andrea Rueda, and Eduardo Romero.
Learning semantic histopathological representation for basal cell carcinoma classification.
In *Proc. of SPIE Vol.*, volume 8676, pages 86760U–1, 2013.
- [23] Le Hou, Dimitris Samaras, Tahsin M Kurc, Yi Gao, James E Davis, and Joel H Saltz.
Patch-based convolutional neural network for whole slide tissue image classification.
In *Proceedings of the IEEE Conference on Computer Vision and Pattern Recognition*, pages 2424–2433, 2016.
- [24] Yongzhen Huang, Zifeng Wu, Liang Wang, and Tieniu Tan.
Feature coding in image classification: A comprehensive study.
IEEE transactions on pattern analysis and machine intelligence, 36(3):493–506, 2014.
- [25] Frederic Jurie and Bill Triggs.
Creating efficient codebooks for visual recognition.
In *Computer Vision, 2005. ICCV 2005. Tenth IEEE International Conference on*, volume 1, pages 604–610. IEEE, 2005.
- [26] Ebrahim Karami, Siva Prasad, and Mohamed Shehata.
Image matching using sift, surf, brief and orb: performance comparison for distorted images.
arXiv preprint arXiv:1710.02726, 2017.
- [27] Meghana Dinesh Kumar, Morteza Babaie, Shujin Zhu, Shivam Kalra, and HR Tizhoosh.
A comparative study of cnn, bovw and lbp for classification of histopathological images.
arXiv preprint arXiv:1710.01249, 2017.
- [28] Sandeep Kumar, Basudev Sharma, Vivek Kumar Sharma, and Ramesh C Poonia.
Automated soil prediction using bag-of-features and chaotic spider monkey optimization algorithm.
Evolutionary Intelligence, pages 1–12, 2018.



Key References V

[29] Manohar Kuse, Tanuj Sharma, and Sudhir Gupta.

A classification scheme for lymphocyte segmentation in h&e stained histology images.

In *Recognizing Patterns in Signals, Speech, Images and Videos*, pages 235–243. Springer, 2010.

[30] Bastian Leibe and Bernt Schiele.

Interleaving object categorization and segmentation.

In *Cognitive Vision Systems*, pages 145–161. Springer, 2006.

[31] Li Li, Lin Feng, Laihang Yu, Jun Wu, and Shenglan Liu.

Fusion framework for color image retrieval based on bag-of-words model and color local haar binary patterns.

Journal of Electronic Imaging, 25(2):023022, 2016.

[32] Yali Li, Shengjin Wang, Qi Tian, and Xiaoqing Ding.

A survey of recent advances in visual feature detection.

Neurocomputing, 149:736–751, 2015.

[33] Wee Loon Lim, Antoni Wibowo, Mohammad Ishak Desa, and Habibollah Haron.

A biogeography-based optimization algorithm hybridized with tabu search for the quadratic assignment problem.

Computational intelligence and neuroscience, 2016:27, 2016.

[34] Wei-Chao Lin, Chih-Fong Tsai, Zong-Yao Chen, and Shih-Wen Ke.

Keypoint selection for efficient bag-of-words feature generation and effective image classification.

Information Sciences, 329:33–51, 2016.

[35] Xi Long, W Louis Cleveland, and Y Lawrence Yao.

A new preprocessing approach for cell recognition.

IEEE Transactions on Information Technology in Biomedicine, 9(3):407–412, 2005.



Key References VI

[36] Haiping Ma.

An analysis of the equilibrium of migration models for biogeography-based optimization.

Information Sciences, 180(18):3444–3464, 2010.

[37] Haiping Ma and Dan Simon.

Blended biogeography-based optimization for constrained optimization.

Engineering Applications of Artificial Intelligence, 24(3):517–525, 2011.

[38] Haiping Ma, Dan Simon, Patrick Siarry, Zhile Yang, and Minrui Fei.

Biogeography-based optimization: a 10-year review.

IEEE Transactions on Emerging Topics in Computational Intelligence, 1(5):391–407, 2017.

[39] Wei-Ying Ma and Bangalore S Manjunath.

Netra: A toolbox for navigating large image databases.

Multimedia systems, 7(3):184–198, 1999.

[40] Christopher Malon, Matthew Miller, Harold Christopher Burger, Eric Cosatto, and Hans Peter Graf.

Identifying histological elements with convolutional neural networks.

In *Proceedings of the 5th international conference on Soft computing as transdisciplinary science and technology*, pages 450–456. ACM, 2008.

[41] Seyedali Mirjalili, Amir H Gandomi, Seyedeh Zahra Mirjalili, Shahrzad Saremi, Hossam Faris, and Seyed Mohammad Mirjalili.

Saltp swarm algorithm: A bio-inspired optimizer for engineering design problems.

Advances in Engineering Software, 114:163–191, 2017.

[42] Seyedali Mirjalili and Andrew Lewis.

The whale optimization algorithm.

Advances in Engineering Software, 95:51–67, 2016.



Key References VII

- [43] Seyedali Mirjalili, Seyed Mohammad Mirjalili, and Andrew Lewis.
Grey wolf optimizer.
Advances in engineering software, 69:46–61, 2014.
- [44] Himanshu Mittal, Raju Pal, Ankur Kulhari, and Mukesh Saraswat.
Chaotic kbest gravitational search algorithm (ckgsa).
In *Contemporary Computing (IC3), 2016 Ninth International Conference on*, pages 1–6. IEEE, 2016.
- [45] Ali W. Mohamed, Anas A. Hadi, Anas M. Fattouh, and Kamal M. Jambi.
LSHADE with semi-parameter adaptation hybrid with CMA-ES for solving CEC 2017 benchmark problems.
In *2017 IEEE Congress on Evolutionary Computation (CEC)*. IEEE, jun 2017.
- [46] Nandita Nayak, Hang Chang, Alexander Borowsky, Paul Spellman, and Bahram Parvin.
Classification of tumor histopathology via sparse feature learning.
In *Biomedical Imaging (ISBI), 2013 IEEE 10th International Symposium on*, pages 410–413. IEEE, 2013.
- [47] Kuan Pei Nei, Stephanie Chua, and Ehfa Bujang Safawi.
A comparative study of features extracted in the classification of human skin burn depth.
Journal of Telecommunication, Electronic and Computer Engineering (JTEC), 9(3-11):47–50, 2017.
- [48] Qun Niu, Letian Zhang, and Kang Li.
A biogeography-based optimization algorithm with mutation strategies for model parameter estimation of solar and fuel cells.
Energy Conversion and Management, 86:1173–1185, oct 2014.
- [49] Stephen O'Hara and Bruce A Draper.
Introduction to the bag of features paradigm for image classification and retrieval.
arXiv preprint arXiv:1101.3354, 2011.

Key References VIII

- [50] SH Ong, XC Jin, R Sinniah, et al.
Image analysis of tissue sections.
Computers in biology and medicine, 26(3):269–279, 1996.
- [51] Silas Nyboe Ørting, Jens Petersen, Laura H Thomsen, Mathilde MW Wille, and Marleen de Bruijne.
Detecting emphysema with multiple instance learning.
In *Biomedical Imaging (ISBI 2018), 2018 IEEE 15th International Symposium on*, pages 510–513. IEEE, 2018.
- [52] Raju Pal and Mukesh Saraswat.
Enhanced bag of features using alexnet and improved biogeography-based optimization for histopathological image analysis.
In *Proc. of Eleventh International Conference on Contemporary Computing, Noida, India, pp. 1–6*, pages 1–6. IEEE, 2018.
- [53] PM Panchal, SR Panchal, and SK Shah.
A comparison of sift and surf.
International Journal of Innovative Research in Computer and Communication Engineering, 1(2):323–327, 2013.
- [54] Xiaojiang Peng, Limin Wang, Xingxing Wang, and Yu Qiao.
Bag of visual words and fusion methods for action recognition: Comprehensive study and good practice.
Computer Vision and Image Understanding, 150:109–125, 2016.
- [55] Hammad A Qureshi, Nasir Mahmood Rajpoot, Tim W Nattkemper, and Volkmar Hans.
A robust adaptive wavelet-based method for classification of meningioma histology images.
2009.
- [56] S Hussain Raza, R Mitchell Parry, Richard A Moffitt, Andrew N Young, and May D Wang.
An analysis of scale and rotation invariance in the bag-of-features method for histopathological image classification.
In *International Conference on Medical Image Computing and Computer-Assisted Intervention*, pages 66–74. Springer, 2011.



Key References IX

[57] Seyed Hamid Rezatofighi and Hamid Soltanian-Zadeh.

Automatic recognition of five types of white blood cells in peripheral blood.

Computerized Medical Imaging and Graphics, 35(4):333–343, 2011.

[58] Monjoy Saha, Chandan Chakraborty, and Daniel Racoceanu.

Efficient deep learning model for mitosis detection using breast histopathology images.

Computerized Medical Imaging and Graphics, 64:29–40, 2018.

[59] Daniel Sanchez-Morillo, Jesús González, Marcial García-Rojo, and Julio Ortega.

Classification of breast cancer histopathological images using kaze features.

In *International Conference on Bioinformatics and Biomedical Engineering*, pages 276–286. Springer, 2018.

[60] Ahmet Saygili, Gunalp Uysal, and Gokhan Bilgin.

Comparative analysis of codeword representation by clustering methods for the classification of histological tissue types.

In *Eighth International Conference on Machine Vision (ICMV 2015)*, volume 9875, page 98750U. International Society for Optics and Photonics, 2015.

[61] Dan Simon.

Biogeography-based optimization.

IEEE transactions on evolutionary computation, 12(6):702–713, 2008.

[62] Neelam Sinha and AG Ramakrishnan.

Automation of differential blood count.

In *TENCON 2003. Conference on Convergent Technologies for the Asia-Pacific Region*, volume 2, pages 547–551. IEEE, 2003.

[63] Korsuk Sirinukunwattana, Shan E Ahmed Raza, Yee-Wah Tsang, David RJ Snead, Ian A Cree, and Nasir M Rajpoot.

Locality sensitive deep learning for detection and classification of nuclei in routine colon cancer histology images.

IEEE transactions on medical imaging, 35:1196–1206, 2016.



Key References X

- [64] Fabio A Spanhol, Luiz S Oliveira, Caroline Petitjean, and Laurent Heutte.
A dataset for breast cancer histopathological image classification.
IEEE Transactions on Biomedical Engineering, 63(7):1455–1462, 2016.
- [65] Umamahesh Srinivas, Hojjat Seyed Mousavi, Vishal Monga, Arthur Hattel, and Bhushan Jayarao.
Simultaneous sparsity model for histopathological image representation and classification.
IEEE transactions on medical imaging, 33(5):1163–1179, 2014.
- [66] Harry Strange and Reyer Zwiggelaar.
Meningioma subtype classification using morphology features and random forests.
In *Medical Imaging 2013: Digital Pathology*, volume 8676, page 86760S. International Society for Optics and Photonics, 2013.
- [67] Nipon Theera-Umporn and Sompong Dhompongsa.
Morphological granulometric features of nucleus in automatic bone marrow white blood cell classification.
IEEE Transactions on Information Technology in Biomedicine, 11(3):353–359, 2007.
- [68] Wei Wang, John A Ozolek, and Gustavo K Rohde.
Detection and classification of thyroid follicular lesions based on nuclear structure from histopathology images.
Cytometry Part A: The Journal of the International Society for Advancement of Cytometry, 77(5):485–494, 2010.
- [69] Wikipedia.
Fermat's Spiral - wikipedia, the free encyclopedia, 12 2017.
- [70] Jun Xu, Lei Xiang, Renlong Hang, and Jianzhong Wu.
Stacked sparse autoencoder (ssae) based framework for nuclei patch classification on breast cancer histopathology.
In *2014 IEEE 11th International Symposium on Biomedical Imaging (ISBI)*, pages 999–1002. IEEE, 2014.



Key References XI

- [71] Jun Xu, Lei Xiang, Qingshan Liu, Hannah Gilmore, Jianzhong Wu, Jinghai Tang, and Anant Madabhushi.
Stacked sparse autoencoder (ssae) for nuclei detection on breast cancer histopathology images.
IEEE transactions on medical imaging, 35(1):119–130, 2016.
- [72] Yungang Zhang, Bailing Zhang, Frans Coenen, and Wenjin Lu.
Breast cancer diagnosis from biopsy images with highly reliable random subspace classifier ensembles.
Machine vision and applications, 24(7):1405–1420, 2013.
- [73] Elizabeth Zimmermann.
Frozen section analysis for breast cancer could save time, anxiety and more than 90 million dollar.
<https://newsnetwork.mayoclinic.org/discussion/>, February 2016.



Thank You

Appendix I

- Standard benchmark functions

Sr. No.	Function Name	Equation	Range	OV	Optimal Position Values	Category
1.	Ackley	$-20e^{-0.02\sqrt{d-1}\sum_{i=1}^dx_i^2}} \\ e^{d-1\sum_{i=1}^d \cos(2\pi x_i)} + 20 + e$	[-35 to 35]	0	(0,...,0)	MM, NS
2.	Alpine	$\sum_{i=1}^d x_i \sin(x_i) + 0.1x_i $	[-10 to 10]	0	(0,...,0)	MM, S
3.	Brown	$\sum_{i=1}^{d-1} (x_i^2)^{(x_{i+1}^2+1)} + (x_{i+1}^2)^{(x_i^2+1)}$	[-1 to 4]	0	(0,...,0)	UM, NS
4.	Levy	$\sin^2(\pi w_1) + \sum_{i=1}^{d-1} (w_i - 1)^2 [1 + 10 \sin^2(\pi w_i + 1)] \\ (w_d - 1)^2 [1 + \sin^2(2\pi w_d)]$, where $w_i = 1 + \frac{x_i - 1}{4}$, for all $i = 1, \dots, d$	[-10 to 10]	0	(1,1,...,1)	MM
5.	New Schwefel	$418.9829d - \sum_{i=1}^d x_i \sin(\sqrt{ x_i })$	[-500 to 500]	0	(420.9687,..., 420.9687)	MM
6.	Pathological	$\sum_{i=1}^{d-1} \left(0.5 + \frac{\sin^2 \sqrt{100x_i^2+x_{i+1}^2} - 0.5}{1 + 0.001(x_i^2 - 2x_i x_{i+1} + x_{i+1}^2)^2} \right)$	[-100 to 100]	0	(0,...,0)	MM, NS
7.	Penalty1	$10 \sin^2(\pi y_1) + \sum_{i=1}^{d-1} (y_i - 1)^2 [1 + 10 \sin^2(\pi y_{(i+1)})] + (y_d - 1)^2 + \sum_{i=1}^d u_i$ where $y_i = 1 + \frac{(x_i + 1)}{4}$, and $u_i = \begin{cases} k(x_i - a)^m & x_i > a \\ 0 & -a \leq x_i \leq a \\ k(-x_i - a)^m & x_i < -a \end{cases}$	[-50 to 50]	0	(1,1,...,1)	MM, NS

Appendix I

- Standard benchmark functions

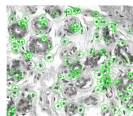
Sr. No.	Function Name	Equation	Range	OV	Optimal Position Values	Category
8.	Penalty2	$\sum_{i=1}^d u_i + 0.1 \left\{ 10 \sin^2(3\pi x_1) + \sum_{i=1}^{d-1} (x_i - 1)^2 [1 + \sin^2(3\pi x_{i+1})] + (x_d - 1)^2 [1 + \sin^2(2\pi x_d)] \right\}$	[-50 - 50]	0	(1,1,...,1)	MM, NS
9.	Powell's First Singular	$\sum_{i=1}^{d/4} (x_{4i-3} + 10x_{4i-2})^2 + 5(x_{4i-1} - x_{4i})^2 + (x_{4i-2} - x_{4i-1})^4 + 10(x_{4i-3} - x_{4i})^4$	[-4 - 5]	0	(0,0,...,0)	UM, NS
10.	Powell's Second Singular	$\sum_{i=1}^{d-2} (x_{i-1} + 10x_i)^2 + 5(x_{i+1} - x_{i+2})^2 + (x_i - 2x_{i+1})^4 + 10(x_{i-1} - x_{i+2})^4$	[-4 - 5]	0	(0,0,...,0)	UM, NS
11.	Powell Sum	$\sum_{i=1}^d x_i ^{i+1}$	[-1 - 1]	0	(0,0,...,0)	UM, S
12.	Quartic	$\sum_{i=1}^d i x_i^4$	[-1.28 1.28]	-	(0,0,...,0)	UM, S
13.	Rastrigin	$10d + \sum_{i=1}^d (x_i^2 - 10\cos(2\pi x_i))$	[-5.12 5.12]	-	(0,0,...,0)	MM
14.	Rotated Hyper-Ellipsoid	$\sum_{i=1}^d \sum_{j=1}^i x_j^2$	[-65.536 65.536]	-	(0,0,...,0)	UM



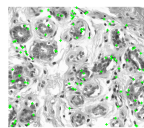
Appendix I

- Standard benchmark functions

Sr. No.	Function Name	Equation	Range	OV	Optimal Position Values	Category
15.	Schwefel	$-\sum_{i=1}^d x_i \sin \sqrt{ x_i }$	[-512 512]	-	0 (420.9687,..., MM, S 420.9687)	
16.	Schwefel3	$\sum_{i=1}^d x_i + \prod_{i=1}^d x_i $	[-10 - 10]	0	(0,0,...,0)	MM, NS
17.	Sphere	$\sum_{i=1}^d x_i^2$	[-5.12 5.12]	-	0 (0,0,...,0)	UM, S
18.	Step	$\sum_{i=1}^d (\lfloor x_i \rfloor)$	[-100 100]	-	0 (0,...,0)	UM, S
19.	Sum Squares	$\sum_{i=1}^d i x_i^2$	[-10 - 10]	0	(0,0,...,0)	UM, S
20.	Trigonometric	$\sum_{i=1}^d [d - \sum_{j=1}^d \cos x_j + i(1 - \cos(x_i) - \sin(x_i))]^2$	[0 - pi]	0	(0,0,...,0)	MM, NS



(a) SURF



(b) ORB

Figure 25: 100 keypoints detected by a) SURF and b) ORB